On the physics of Trotterization

THESIS

submitted in partial fulfillment of the
requirements for the degree of

BACHELOR OF SCIENCE
in
PHYSICS

Author :	Tobias Göbel
Student ID :	s2052121
Supervisor :	Dr. V. Cheianov
In collaboration with :	M.Sc. Y. Herasymenko
2^{nd} corrector :	Dr. T.E. O'Brien

Leiden, The Netherlands, June 19, 2020

On the physics of Trotterization

Tobias Göbel

Huygens-Kamerlingh Onnes Laboratory, Leiden University
P.O. Box 9500, 2300 RA Leiden, The Netherlands

June 19, 2020

Abstract

Quantum computing is a new mode of computation that allows qualitative advantage over classical computers for certain tasks. One such task is calculating the lowest energy states of quantum systems. In the near term, a promising quantum algorithm for this task is the variational quantum eigensolver (VQE). In order to realize a VQE, one needs to choose a good ansatz for the ground state. The accuracy of the approximation of the VQE essentially depends on the chosen ansatz. Motivated by unitary coupled cluster (UCC) theory in quantum chemistry, the UCC-ansatz has emerged as a standard in the context of VQEs. Implementation on a quantum circuit for this ansatz however, requires a Suzuki-Trotter approximation. In this thesis, we identify two key approaches in this "Trotterization" method. We investigate the behaviors of the resulting Trotterization schemes. We found a drastic, system-dependent variation in the performances of the different Trotterization schemes. Therefore we recognize that the choice of Trotterization scheme might be crucial for quantum advantage in the near future. Based on the analysis in this research, we propose a system-adapted criterion for efficient Trotterization choice. On top of that, we suggest a new VQE ansatz. For certain systems, this ansatz approximates the ground state considerably more accurately than the other ansatzes considered in this project.

Contents

Version of June 19, 2020– Created June 19, 2020 - 18:30

Version of June 19, 2020– Created June 19, 2020 - 18:30

Chapter 1

Introduction

The rise of quantum theory during the twentieth century has profoundly changed our understanding of physics. The theory provided solutions to inexplicable phenomena and predicted the existence of unseen physical situations. Describing systems quantum mechanically turned out to be of great value to both science and technology. To characterize physics on a new level of accuracy, quantum mechanical systems are also being studied with computer simulations. However, when one expands the size of simulated quantum systems, the computational limits of the computing hardware are quickly reached [1]. This problem is related to the fact that exponentially more information is required to describe a quantum mechanical state, compared to the classical one. In an attempt to solve this problem, the concept of a quantum computer emerged [1]. With this technique, a controllable quantum system is used to simulate other quantum mechanical systems. The quantum mechanics is therefore already embedded into the computer itself. Consequently, the requirement for exponentially growing computational resources is avoided. Therefore, the quantum computer is able to solve certain problems exponentially faster compared to the classical computer. At this moment in time however, quantum computers are practically hard to build. Quantum hardware tends to equilibrate with its surroundings easily, losing its capabilities as a result. This strictly limits the time current quantum computers can operate. In this early period of quantum hardware development [2], the new, more appropriate algorithms are needed. The present thesis focuses on optimizing one such algorithm: variational quantum eigensolver [3].

1.1 The variational quantum eigensolver (VQE)

Obtaining ground states is crucial for studying quantum mechanical systems. Ground states contain a lot of information about the physics of the system, but tend to get computationally expensive to calculate as the size of the system increases. A promising class of quantum algorithms for approximating ground states are variational quantum eigensolvers (VQEs) [3]. These algorithms consist of a combination of quantum and classical algorithm. The length of the quantum circuit is generally relatively short, such that it is one of the most competitive algorithms to be applied on near term quantum devices.
VQEs typically contain a quantum device, on which a set of parametrized unitary gates $U(\vec{\theta})$ act on an initial state $|0\rangle$. The unitary gates are adjustable by changing the parameters $\vec{\theta}$. Thereafter, the expectation value of the energy $\langle \Psi_{res}(\vec{\theta})| \hat{H} |\Psi_{res}(\vec{\theta})\rangle$ is measured. Then, the classical algorithm tries to optimize the parameters $\vec{\theta}$ in order to obtain the state with the lowest energy. This is done using a standard minimization algorithm. Small adjustments to the parameters $\vec{\theta}$ are made until a minimum is found. In this way, the VQE approximates the ground state of the system.

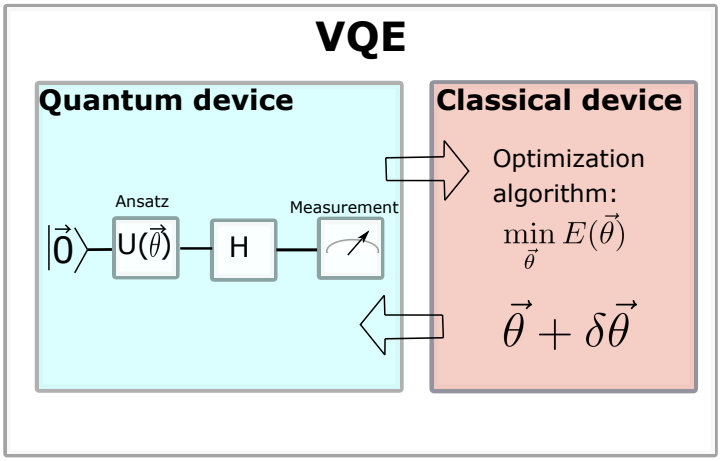

Figure 1.1: *Schematic overview of the VQE. The quantum device prepares a quantum state $U(\vec{\theta})\,|\vec{0}\rangle$. The energy of this state is measured, and given to the classical device. An optimization algorithm returns an adjustment $\delta\vec{\theta}$ to the quantum device. This process repeats until a minimum energy is found.*

Version of June 19, 2020– Created June 19, 2020 - 18:30

1.2 Unitary coupled cluster ansatz (UCC)

The set of unitary gates, or the ansatz, that is used in the VQE, determines what part of the Hilbert space can be searched through. Since one can typically only search through a small part of the total Hilbert space, one must choose the ansatz thoughtfully depending on the system. A class of ansatzes frequently used in quantum chemistry, is the unitary coupled cluster ansatz (UCC) [3, 4]. UCC is proven to satisfy the linked cluster theorem [5], which is a benefit as it assures the ability to reproduce perturbation theory. The UCC ansatz is of the form:

$$U(\vec{\theta}) = e^{\sum_j \theta_j \hat{O}}, \theta_j \in \mathbb{R} \tag{1.1}$$

Where $\hat{O}$ can be chosen to be any anti-hermitian operator. Since the pauli-operators σ_x, σ_y and σ_z are all hermitian, $i\sigma_x$, $i\sigma_y$ and $i\sigma_z$ are all anti-hermitian. Therefore the expression above can be rewritten as:

$$U(\vec{\theta}) = e^{\sum_j \theta_j (iP_j)}, \theta_j \in \mathbb{R} \tag{1.2}$$

P is a Pauli-string of the form $\bigotimes_{j=1}^{N} \sigma_j$ where $\sigma_j \in \sigma_x, \sigma_y, \sigma_z, I$.

1.3 Trotterization

Implementing UCC on a quantum device requires an approximation by a so called Trotter-Suzuki method [6, 7]. Quantum gates do not allow for superpositions of Pauli operators. The UCC-ansatz as given in eq. (1.2) is therefore not realizable onto a quantum circuit, as a sum of Pauli operators appears in the exponential. Because the Pauli-strings in the exponential do not necessarily commute, one cannot simply rewrite as a product of exponentials. Instead, a Trotter-Suzuki method is required.

$$e^{\sum_j \hat{O}_j} = \lim_{\rho \to \infty} (\Pi_j e^{\hat{O}_j/\rho})^\rho \tag{1.3}$$

When applied to the UCC ansatz, we obtain:

$$U(\vec{\theta}) = \lim_{\rho \to \infty} (\Pi_j e^{i\theta_j P_j/\rho})^\rho \tag{1.4}$$

Although this expression is now rewritten as a product of unitary operators, it is still not realizable on a quantum circuit, because this expression

Version of June 19, 2020– Created June 19, 2020 - 18:30

would require an infinite amount of gates. Hence, an approximation is needed.

$$\tilde{U}(\vec{\theta}) = (\Pi_j e^{i\theta_j P_j/\rho})^\rho \approx e^{\sum_j \theta_j (iP_j)}, \rho \in \mathbb{N} \tag{1.5}$$

The number ρ is finite at this point and is called the Trotter-number. The ansatz $\tilde{U}(\vec{\theta})$ is realizable on a quantum device, but no longer equals the original UCC-ansatz.

In the context of VQEs, one might improve this ansatz by relaxing the parameters for each separate unitary operator [3]:

$$\tilde{U}^*(\vec{\theta}) = \Pi_i^\rho \Pi_j e^{i\theta_{i,j} P_j}, \rho \in \mathbb{N} \tag{1.6}$$

The $\tilde{U}^*(\vec{\theta})$ ansatz is essentially similar to the $\tilde{U}(\vec{\theta})$ ansatz, but all exponentials in the $\tilde{U}^*(\vec{\theta})$ ansatz have an independent parameter θ. Whereas the parameters of the $\tilde{U}(\vec{\theta})$ ansatz are repeated along the different Trotter-steps. So, since $\tilde{U}^*(\vec{\theta})$ is parametrized by more parameters, the part of the Hilbert space that is covered by $\tilde{U}^*(\vec{\theta})$ completely contains, and is bigger than the space covered by $\tilde{U}^(\vec{\theta})$. Therefore the performance of $\tilde{U}^*(\vec{\theta})$ is equal or better than the performance of $\tilde{U}(\vec{\theta})$. This is an improvement at low cost, as the number of gates is maintained.

1.4 Generators

To further specify the UCC ansatz, a set of generators is required. These generators determine what part of the Hilbert space can be searched through. Evidently, the optimal set of generators therefore depends on the nature of the problem. In this project, we select the set of generators based on perturbation theory [8]. In order to do so, we first narrow down the class of problems to spin systems of size N. The Hamiltonians of these systems are of the following form:

$$H = H_0 + JV = -h \sum_i^N \sigma_i^z - J \sum_j P_j \tag{1.7}$$

Here σ_i^z applies an Pauli-z operator on the i^{th} particle, and identity operators on the remaining particles: $\sigma_i^z = I_1 \bigotimes I_2 ... \bigotimes \sigma_i^z \bigotimes ... \bigotimes I_N$. P is a Pauli-string of the form $\bigotimes_{j=1}^N \sigma_j$ where $\sigma_j \in \sigma_x, \sigma_y, \sigma_z, I$. The term $J \sum_j P_j$, also JV, is considered as a perturbation to H_0. The unperturbed ground-state of this class of systems is $|\vec{0}\rangle$ with $E = -hN$.

Version of June 19, 2020– Created June 19, 2020 - 18:30

$$H_0 |\vec{0}\rangle = -hN |\vec{0}\rangle$$

Building from this state, generators are chosen based on terms appearing in perturbation theory. Terms in perturbation theory can be reproduced by a diagrammatic method. The diagrams depict the action of coupling terms P_i on the spin particles. We consider combinations of couplings $\vec{k}$, where the value of the i^{th} entry of $\vec{k}$ represents how many times the coupling P_i is activated [8]. The action of the activated couplings on the initial state $|\vec{0}\rangle$, produces a state $|\vec{s}(\vec{k})\rangle$ that appears as a contribution in perturbation theory.

$$\Pi_i P_i^{k_i} |\vec{0}\rangle = i^{\Gamma(\vec{k})} |\vec{s}(\vec{k})\rangle$$

Where $\Gamma(\vec{k}) \in \{0, 1, 2, 3\}$ determines the phase created by $\vec{k}$. Thereafter, generators $G(\vec{k})$ are chosen such that these states are reproduced by the corresponding gates $iG(\vec{k})$.

$$iG(\vec{k}) |\vec{0}\rangle = \pm i^{a(\vec{k})} |\vec{s}(\vec{k})\rangle \tag{1.8}$$

Where $a \in \{0, 1\}$. Generators are only required to depend on $a(\vec{k})$, as the parametrized gate in the VQE is able to cover both positive and negative values.

$$e^{i\theta G(\vec{k})} = \cos(\theta) I + i \sin(\theta) G(\vec{k})$$

In order to reproduce the state $|\vec{s}(\vec{k})\rangle$, $G(\vec{k})$ consists of $\sigma_x = X$ operators used to flip the desired qubits. If $a(\vec{k}) = 0$ however, the first nontrivial operator is given by an $\sigma_y = Y$ operator. So if $a(\vec{k}) = 1$, $G(\vec{k})$ is given by:

$$G(\vec{k}) = X_1^{s(\vec{k})_1} \bigotimes ... \bigotimes X_N^{s(\vec{k})_N}$$

Note that Pauli matrices are involutary, such that $P^2 = I$. If $a(\vec{k}) = 0$, with the first nontrivial gate at position α, $G(\vec{k})$ is given by:

$$G(\vec{k}) = I_1 \bigotimes ... \bigotimes Y_\alpha \bigotimes X_{\alpha+1}^{s(\vec{k})_{\alpha+1}} \bigotimes .... \bigotimes X_N^{s(\vec{k})_N}$$

Constructing $G(\vec{k})$ in this systematic way, assures that eq. 1.8 is satisfied.

Moreover, the sum of the components of $\vec{k}$, $\sum_i k_i$, corresponds to the order of the contribution in perturbation theory. In this way, a natural order of importance arises: Generators are chosen in ascending order of $\sum_i k_i$.

Every $\vec{k}$ can be depicted in a diagram to make contributions more visual. A diagram consists of N dots on a horizontal line, which represent the qubits acted upon. The dot is colored black if the respective qubit is flipped with respect to the initial state $|\vec{0}\rangle$. Or in other words, qubit i is pictured black if $s(\vec{k})_i = 1$. Otherwise, the dot is colored white. The activated couplings as given by $\vec{k}$, are depicted as squares. Lines are drawn, connecting the squares to the qubits on which is acted. A blue line represents a X coupling, a red line represents a Y coupling and a black line represents a Z coupling.

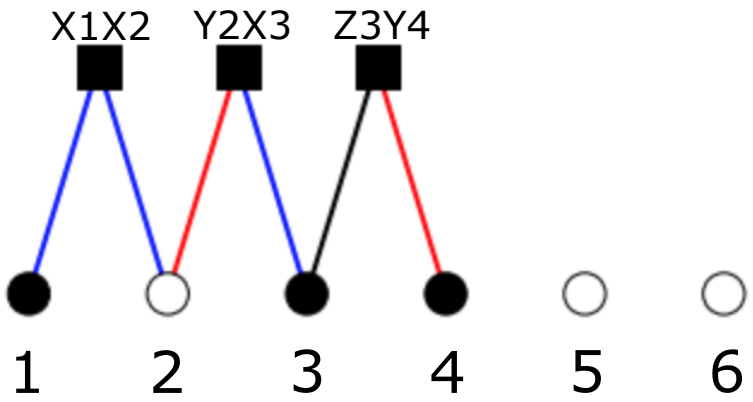

Figure 1.2: *Example of a diagram. On a $N = 6$ qubit system, three couplings are activated: X1X2, Y2X3 and Z3Y4. This combination of couplings flips the first, the third and the fourth qubit. Therefore, $|\vec{s}(\vec{k})\rangle = |101100\rangle$. The numbering of the qubits and the coupling terms are shown for reference, but are unnecessary.*

Not every combination of couplings $\vec{k}$ corresponds to a generator that needs be included in the generator set. If $\vec{k}$ is either subleading or disconnected, other generators make up for its contribution. Therefore we are not required to include these gates in order to reach the ground state according to perturbation theory.
We define $\vec{k^a}$ to be subleading if the corresponding state $|\vec{s}(\vec{k^a})\rangle$, is also produced by another combination of couplings $\vec{k^b}$, which is lower in order of perturbation theory: $\sum_i k_i^b < \sum_i k_i^a$.

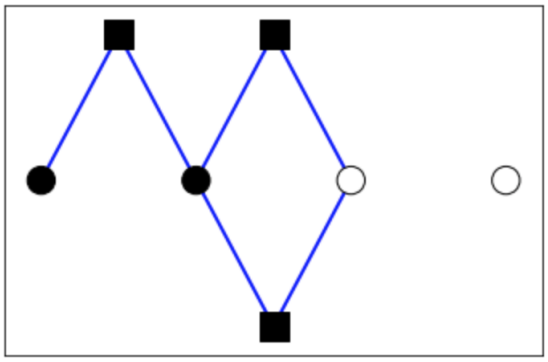

Figure 1.3: *Example of a subleading contribution. If we consider the couplings* $\{X1X2, X2X3, X3X4\}$*, this diagram corresponds to* $\vec{k} = (1,2,0)$*. The order in perturbation theory of this contribution is* $\sum_i k_i = 3$*. The state produced by this diagram* $|\vec{s}(\vec{k})\rangle = |1100\rangle$ *however, is similar to the state produces by* $\vec{k} = (1,0,0)$*. Since this contribution has a lower order of perturbation theory, the depicted diagram is subleading.*

We define $\vec{k}$ to be disconnected, if $\vec{k}$ can be written as $\vec{k} = \vec{k_A} + \vec{k_B}$, where $\vec{k_A}$ and $\vec{k_B}$ do not act upon any common qubits. The contribution connected to $\vec{k}$ is compensated by the product of the contributions of $\vec{k_A}$ and $\vec{k_B}$.

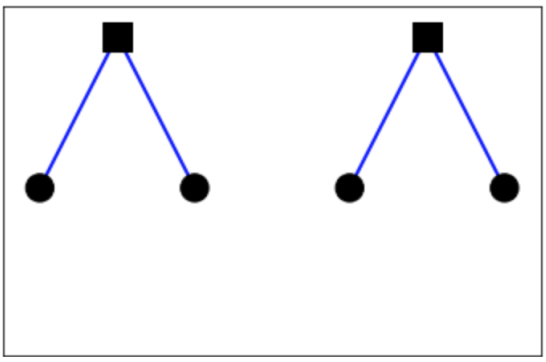

Figure 1.4: *Example of a disconnected contribution. Again, we consider the couplings* $\{X1X2, X2X3, X3X4\}$*. The diagram then corresponds to* $\vec{k} = (1,0,1)$*. We can rewrite as a sum:* $\vec{k} = (1,0,1) = (1,0,0) + (0,0,1)$*.* $\vec{k_A} = (1,0,0)$ *acts upon qubit 1 and qubit 2, whereas* $\vec{k_B} = (0,0,1)$ *acts upon qubit 3 and qubit 4. Following the definition, we conclude that the contribution in the figure is disconnected.*

1.5 Two tendencies

The Trotterized version of the UCC-ansatz, as described in equation (1.6), is not completely specified yet. When considering a fixed amount of gates, one can either choose to approximate the UCC ansatz by selecting certain gates and repeat those among multiple Trotter steps, or one could use all different gates, using only one Trotter step.

$$\tilde{U}^*(\vec{\theta}) = \Pi_i^{\rho} \Pi_j^{N_p} e^{i\theta_{i,j} P_j}, \rho \in \mathbb{N}, N_p \in \mathbb{N} \tag{1.9}$$

Here N_p is the size of the considered gate set. ρ represents the number of Trotter steps. The product of the two, $N_p\rho$, equals the total amount of gates on the VQE circuit. The required coherence time of a quantum algorithm is related to the total number of gates on the respective quantum circuit. Limited coherence time is one of the main complications to near-term quantum computers. Therefore, ansatzes with equal amount of gates are compared. Since a fixed amount of gates requires the product $N_p\rho$ to be constant, we can identify two tendencies in Trotterizing the UCC ansatz: Either selecting a high ρ and low N_p or vice versa.

1.6 This research

In this project we study UCC-based ansatz structures in the context of VQEs. Ansatzes are described by two basic elements: the ansatz generators and the choice of Trotterization scheme. We determine the selection of generators based on perturbation theory, which is a standard approach in quantum chemistry. In this project, a Python module is created that outputs generators up to a desired order in perturbation theory, depending on a given Hamiltonian. With the generator choice being automated by this Python module, we focus on studying the behaviors of different Trotterization schemes. Two key tendencies in these Trotterization schemes are identified: Either use one Trotter step $\rho = 1$, or use multiple Trotter steps, only repeating first order gates. Although both tendencies are approximations to the UCC ansatz, we expect them to behave differently. As we try to confirm this hypothesis, we also investigate which tendency is most efficient, depending on the considered system. The results show that the choice of Trotterization scheme induces drastically different performances. For larger systems, the choice of Trotterization scheme will therefore be decisive for quantum advantage in the near future. With both numerical

and analytical analysis, we examine the behaviors of these Trotterization schemes. Building upon this analysis, a system-adapted criterion for an efficient Trotterization choice is provided. We also introduce a new hybrid ansatz, which combines the two Trotterization tendencies. For certain models, this ansatz is found to perform considerably better compared to the other ansatzes.

Chapter 2

Methods

2.1 Models

In order to study the different ansatzes, we apply the ansatzes on three different one-dimensional spin-systems. All of which are described by a Hamiltonian that consists of a non-interacting part and an interacting part. The interacting part V is considered as the perturbation to the non-interacting part H_0. See equation (1.7).

2.1.1 TFIM

The first model we consider is the transverse field Ising model (TFIM). The interacting part of the Hamiltonian consists of x-x couplings to all neighbors. The Hamiltonian is given by:

$$H = -\sum_{i}^{N} \sigma_i^z - J \sum_{i}^{N-1} \sigma_i^x \sigma_{i+1}^x \tag{2.1}$$

The value J determines the strength of the interacting contributions to the Hamiltonian. For the sake convenience, we have set the value of h, as given in eq. (1.7), to 1. In all models, we use an open boundary condition.

2.1.2 AHM

We also consider the anistropic Heisenberg model (AHM). This model adds a z-z coupling to the TFIM, such that he interacting part of the Hamiltonian consists of x-x and z-z couplings to all neighbors. The Hamiltonian

is given by:

$$H = -\sum_{i}^{N} \sigma_i^z - \frac{J}{2} \sum_{i}^{N-1} (\sigma_i^x \sigma_{i+1}^x + \sigma_i^z \sigma_{i+1}^z) \tag{2.2}$$

2.1.3 NTFIM

The last model we use in this project is the non-transverse field Ising model (NTFIM). This model can be seen as a TFIM, but with a tilted magnetic field acting on the spins. The interacting part of the Hamiltonian consists of (x+z)(x+z) couplings to all neighbors. The total Hamiltonian is written as follows:

$$H = -\sum_{i}^{N} \sigma_i^z - \frac{J}{2} \sum_{i}^{N-1} (\sigma_i^x + \sigma_i^x)(\sigma_{i+1}^z + \sigma_{i+1}^z) \tag{2.3}$$

2.1.4 Gapped and Gapless systems

Depending on the coupling strength, these models can be subdivided into either gapped or gapless models. In our analysis, this turned out to be a useful distinction, since the performances of the ansatzes showed to be related to this classification.

As the coupling strength J of a system increases, the ground state and the ground energy typically change. For gapped systems, the change of the ground state as J increases, $\frac{d\Psi}{dJ}$, is perturbatively small [9]. A system is defined as gapped if the difference between the two lowest energies, corresponding to eigen states, is nonzero for infinite system size: $E_2 - E_1 = \Delta E > 0, N \to \infty$. We define a system to be gapless if either $\Delta E = 0$ or if $\Delta E = 0$ for $N \to \infty$. While the coupling is gradually increased, gap closing might occur at a specific coupling J. Gap closing takes place if a gapped system transforms into a gapless system. This particular value of J at which this occurs, is also called the critical point. At such a point, the ground state changes drastically as the coupling J increases. This transition has implications on the effectiveness of perturbation theory. The radius of convergence of perturbation theory depends on the ground state gap ΔE, which is zero or shrinks algebraically with the system size for gapless systems. Therefore, perturbation theory collapses completely after the gap closing. Perturbation theory is based on the unperturbed ground state, but the ground state after the critical point, $J > J_{critical}$, differs substantially. In this case, the usage of the perturbative method for

Version of June 19, 2020– Created June 19, 2020 - 18:30

choosing generators will be less effective. For some models however, the critical point does not exist. In this case, the ground state Ψ only changes gradually as the coupling J increases. We say the ground state is adiabatically connected to the unperturbed ground state. This suggests the use of cluster analysis to be efficient. Since the ground state remains similar to the reference state, we expect perturbation theory motivated ansatzes to perform well, even in strongly coupled regimes.
From the models that are considered in this project, gap closing only occurs for the transverse field Ising model (TFIM). The critical point is given by: $J_{critical} = 1$. Both AHN and NTFIM are gapped for all finite values of coupling J.

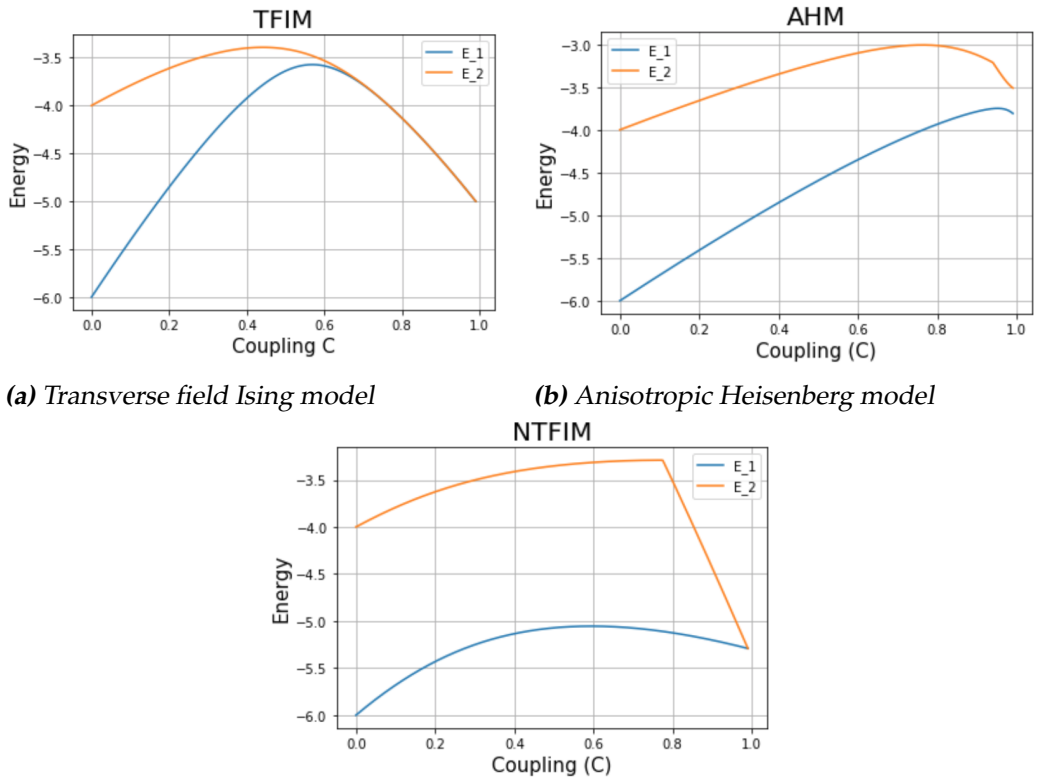

(a) *Transverse field Ising model*

(b) *Anisotropic Heisenberg model*

(c) *Non-transverse Field Ising model*

Figure 2.1: *Lowest two energies for the different $N = 6$ spin systems, as the coupling C increases. Note that the energy is re-scaled, with $H = (C-1)H_0 + CV$. So, $C = 0$ corresponds to $H = H_0$. Where $C = 1$ yields $H = V$.* ***(a):*** *For TFIM, the lowest two energies merge around $C = 0.5$ or $J = 1$.* ***(b):*** *For AHM, the system remains gapped for every value of C.* ***(c):*** *For NTFIM, the gap does not close until C approaches 1, which corresponds to $J \to \infty$.*

2.2 Python module

To systematically calculate the generator set depending on the given Hamiltonian, a python module is written. The generators are calculated with the method described in section (1.4). Depending on the system, gates that directly correspond to terms in perturbation theory, are chosen. This process is automated with a python module, which will be described in this section.

2.2.1 Input

The required input of the python module is given by the following objects:

- **N**; The number of spin-particles
- **Interactions**; Only the interacting part of the Hamiltonian needs to be given, as the non-interacting part is invariant. These interactions are represented in a Python list with following format:

  $$interactions = [[''P_1^1 1 P_2^1 2 ... P_N^1 N'', J^1], [''P_1^2 1 P_2^2 2 ... P_N^2 N'', J^2], ..., [''P_1^L 1 P_2^L 2 ... P_N^L N'', J^L]]$$

  Where P_i^j is one of the Pauli-matrices X, Y, Z or I, applied to the i^{th} qubit. L is the total number of interactions and N the amount of qubits. J^j represents the coefficient of the j^{th} interaction as the order of the list suggests. To make things shorter and more convenient, one can leave identities acting on qubits out of the expression. The interactions of a 4-qubit TFIM system might be given as:

  $$interactions = [[''X1X2'', J], [''X2X3'', J], [''X3X4'', J]]$$

- **PT-order**; A number that determines up to which order in perturbation theory generators need to be considered.
- **P-n**; The number of generators that need to be returned.

2.2.2 Output

With this input, the module can return the following objects:

- **The generators**; P-n different generators, represented as matrices of size 2^N.

Version of June 19, 2020– Created June 19, 2020 - 18:30

- **Diagrams**; A set of P-n different diagrams to visualize the generators.

- **Cirq Circuit**; A quantum circuit with the respective generators, built with the cirq module.

2.2.3 The code

First, all combinations of coupling combinations $\vec{k}$ with length L are produced. We restrict the values of all entries to be smaller or equal than 2, such that: $k_i \leq 2 \; \forall i$. Because Pauli operators are involutory, which means that $PP = I$, applying a coupling twice is similar to applying the identity operator. But since applying a coupling twice might make a diagram connected, these actions need to be considered. If any value of $\vec{k}$ exceeds 2 however, the corresponding contribution is guaranteed to be subleading.

Thereafter, we loop through these $\vec{k}$ vectors in ascending order of $\sum_i k_i$. Note that the list contains $\vec{k}$ vectors up to $\sum_i k_i =$ PT-order and has exactly P-n elements. For each $\vec{k}$ we then check whether its contribution is either subleading or disconnected. If neither subleading nor disconnected, the $\vec{k}$ is added to a separate list, only containing $\vec{k}$ vectors that need to be considered for building the generator set. Every $\vec{k}$ vector in this list must produce a different state $i^{a(\vec{k})} \, |\vec{s}(\vec{k})\rangle$, such that all contributions are leading.
For each contributing $\vec{k}$, a diagram is drawn. See fig. (1.2), (1.3) and (1.4). $|\vec{s}(\vec{k})\rangle$ is determined, after which the flipped qubits are colored black. The couplings are depicted as squares with lines towards the coupled qubits.
The connected and leading $\vec{k}$ vectors are also mapped to a list of generators $G(\vec{k})$ using the method as described in the introduction. With these generators, the parametrized matrix representations of the unitary gates can be obtained. By optimizing the parameters, one can simulate the performance of a VQE. The code is also able to implement the gates on a cirq quantum circuit.

Version of June 19, 2020– Created June 19, 2020 - 18:30

2.2.4 Overview

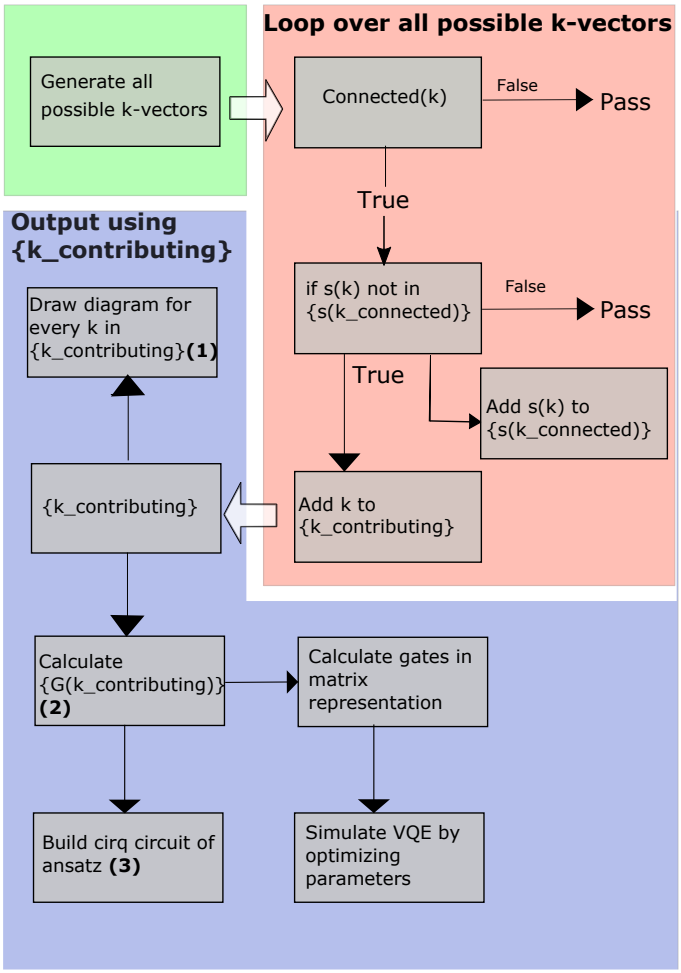

Figure 2.2: *Block scheme of the python module. First, in the green box, every $\vec{k}$ of length L is generated. Some of these $\vec{k}$ vectors might correspond to a subleading or disconnected contribution. In the red box, only leading and connected $\vec{k}$ vectors are selected, and put into the list $\{k_{contributing}\}$. This is done by looping over all possible $\vec{k}$ vectors, in ascending order of $\sum_i k_i$. First a check for connectedness is applied, after which the code determines whether the state $i^{a(\vec{k})}\,|\vec{s}(\vec{k})\rangle$ has not already been occupied by a $\vec{k}$ of lower order. This process assures the $\vec{k}$ vectors, that are added to $\{k_{contributing}\}$, to be leading. From $\{k_{contributing}\}$ three different outputs are constructed.* ***(1)****: For every contributing $\vec{k}$, the code produces a diagram.* ***(2):*** *$\{k_{contributing}\}$ is mapped to a list of generators. The mapping prodedure is described in section (1.4). With the choice of a Trotterization scheme, the generators can either be mapped to a cirq quantum circuit* ***(3)****, or to a matrix representation of the ansatz.*

2.3 Ansatzes

With the generator set being set, we need to choose different Trotter structures in order to specify the ansatzes. We mainly focus on the two tendencies as identified in the introduction. In this section, we formulate the ansatzes representing these tendencies.

2.3.1 QCA

The QCA ansatz [8] is a UCC-based Trotterization like equation (1.8), but with only one Trotter step.

$$U_{QCA}(\vec{\theta}) = \Pi_i^{N_p} e^{i\theta_i P_i} \tag{2.4}$$

This implies that the ansatz consists of N_p different gates, each with an independent parameter. QCA satisfies the linked cluster theorem [8], and therefore is proven to be able to recover the ground state according to perturbation theory.
As all gates are different, high order gates tend to get non-local with this ansatz. Non-local gates are generally undesirable since it is practically hard to perform non-local operations using quantum computers. In principle, one could decompose non-local gates into sets of local gates. Where the depth of a set scales with the number of qubits in between the coupled qubits. Hence, the QCA in this form is a hardware inefficient ansatz.

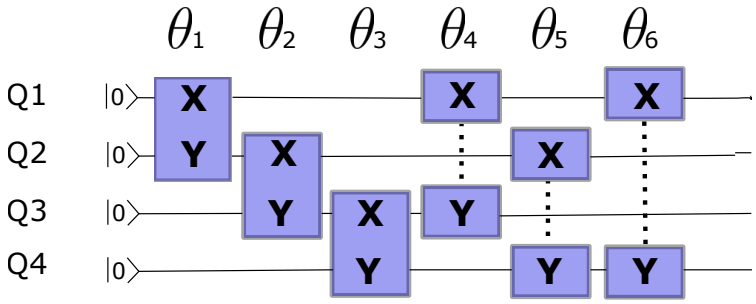

Figure 2.3: *Example of QCA on a quantum circuit. This QCA is designed for a $N = 4$ TFIM system. 6 different gates are shown, all parametrized by an angle θ_i.*

2.3.2 TUCC

The TUCC ansatz is a Trotterization of UCC, with a large Trotter number. Only the first-order gates in perturbation theory are included and then repeated.

Version of June 19, 2020– Created June 19, 2020 - 18:30

$$U_{TUCC}(\vec{\theta}) = \Pi_j \Pi_i^{N_{first}} e^{i\theta_{i,j} P_i} \tag{2.5}$$

Where N_{first} is the number of first-order gates in perturbation theory. This ansatz does not satisfy the linked cluster theorem. Consequently, there is no guarantee that the ground state according to perturbation theory can be acquired.
The first-order gates in perturbation theory are typically acting on neighboring qubits. Therefore, TUCC tends to have less non-local gates compared to QCA, such that TUCC is more hardware efficient ansatz.

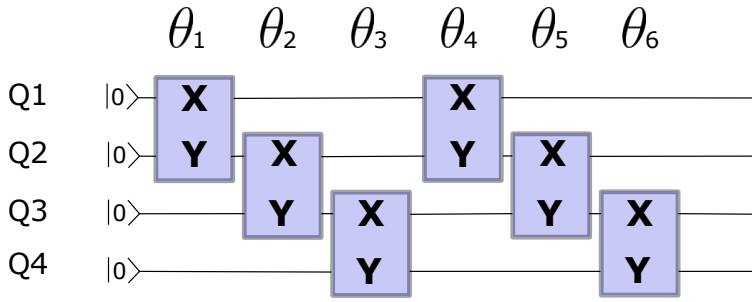

Figure 2.4: *Example of TUCC on a quantum circuit. This TUCC ansatz is designed for a $N = 4$ TFIM system. 2 Trotter steps of the lowest order gates in perturbation theory, together make 6 gates. Each parametrized by an angle θ_i.*

Version of June 19, 2020– Created June 19, 2020 - 18:30

Chapter 3

Study of Trotterization

In this section the behaviors of the defined ansatzes are studied. We simulate the functioning of a VQE by evaluating the action of the quantum circuit classically. The errors in the energy that are produced by these VQEs are plotted against the number of gates, such that the efficiency of the respective ansatzes can be compared. In addition, we investigate the functioning of the ansatzes by examining how the parameters change as more gates are used. Based on this analysis, we present a heuristic about the nature of the different ansatzes, provided with a numerical experiment. At last, we suggest to combine two ansatzes into a new ansatz and review its performance.

3.1 Analysis

3.1.1 General performance features

We measure the performance of an ansatz by considering the error $\epsilon = \frac{E_{VQE} - E_{exact}}{E_{exact}}$. Where E_{VQE} is calculated by simulating the VQE ansatz. E_{exact} is the exact ground energy of the system. From the figures, one can see that the error shrinks or remains equal with the addition of a new gate. This is not surprising, as the space that can be searched through is similar if the new parameter is set to zero. If the new parameter is allowed to change however, the performance can only improve.
Furthermore, a pattern of step-wise improvement in the performance can be recognized. The error seems to decrease in steps of variable length, as more gates are added. This can be explained from the observation that

the k^{th} step corresponds to the gates that are responsible for all k^{th} order contributions in perturbation theory.

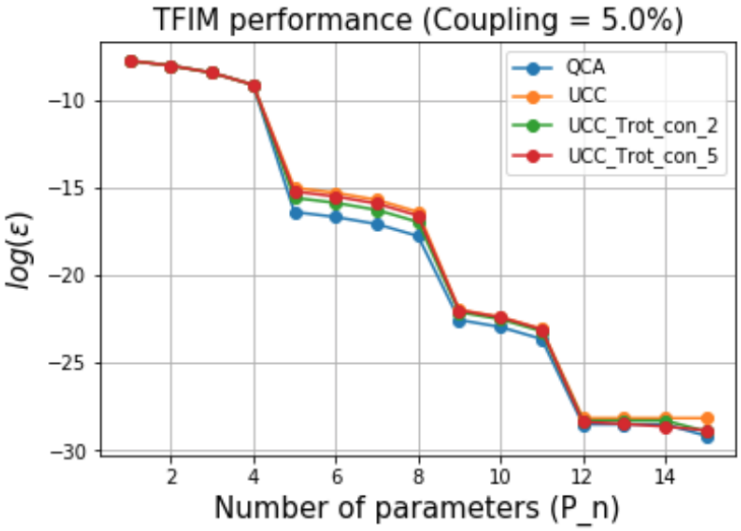

Figure 3.1: *Example of a performance plot. In this figure one can see the natural logarithm of the error $log(\epsilon)$ of different ansatzes as a function of the number of parameters. The ansatzes in this plot are QCA (blue line), UCC (orange line), the constrained version of UCC with 2 Trotter steps (UCC_Trot_con_2) (green line) and the UCC_Trot_con_5 (red line). These ansatzes are applied on a $N = 6$ TFIM system with a coupling strength of 5% relative to the total Hamiltonian ($C = 0.05$).*

3.1.2 Trotter advantage

First, we examine the performance of the orignal UCC-ansatz relative to constrained UCC Trotterizations with various Trotter numbers. The constrained UCC Trotterization are constructed of $P_n\rho$ gates with only P_n independent parameters. See equation (1.5). Although the original UCC-ansatz cannot be realized onto a quantum circuit, it is possible to evaluate its performance classically. Since the Trotterizations are approximations to the original UCC-ansatz, they are expected to perform differently. There is no guarantee, however, that UCC will outperform the Trotterized versions. In fact, the Trotterizations outperform the original UCC-ansatz. More specifically, ansatzes with a low Trotter number typically perform best. This suggests that the back-action among the generators, introduced by the Trotterization, has a positive effect on the performance.

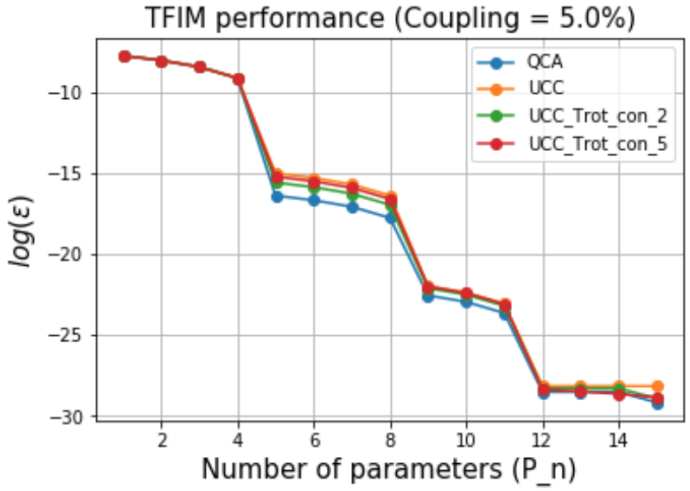

(a) *Transverse field Ising model*

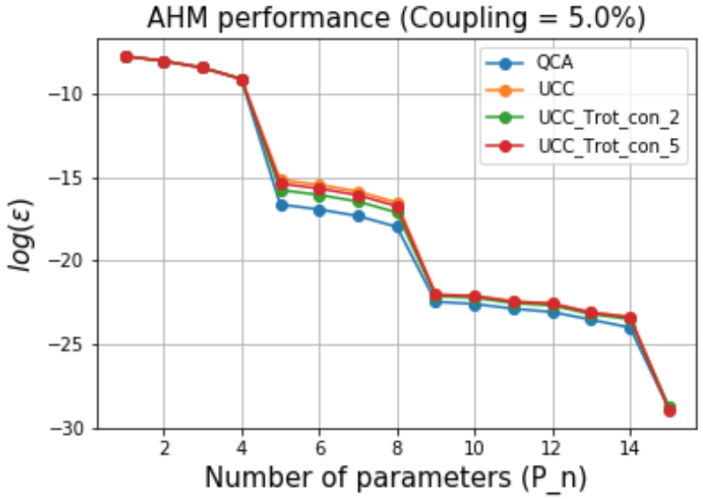

(b) *Anisotropic Heisenberg model*

Figure 3.2: *In this figure one can see the natural logarithm of the error $log(\epsilon)$ of different ansatzes as a function of the number of parameters. The ansatzes in this plot are QCA (blue line), UCC (orange line), the constrained version of UCC with 2 Trotter steps (UCC_Trot_con_2) (green line) and the UCC_Trot_con_5 (red line). In figure* ***(a)****, these ansatzes are applied on a $N = 6$ TFIM system with a coupling strength of 5% relative to the total Hamiltonian. In figure* ***(b)****, a $N = 6$ AHM system with 5% coupling is considered ($C = 0.05$).*

3.1.3 Performance comparison QCA and TUCC

In this project, we mainly investigate the behaviors of QCA and TUCC, as they represent the two UCC Trotterization tendencies. Based on the theory given in the introduction, we expect QCA to perform best for weakly coupled models. Ground states of weakly coupled systems are accurately described by perturbation theory, such that QCA is guaranteed to perform well. Perturbation theory is considered to be inapplicable for gapless systems, where we expect QCA to be less efficient, as the ground state is adiabatically disconnected from the unperturbed ground state.

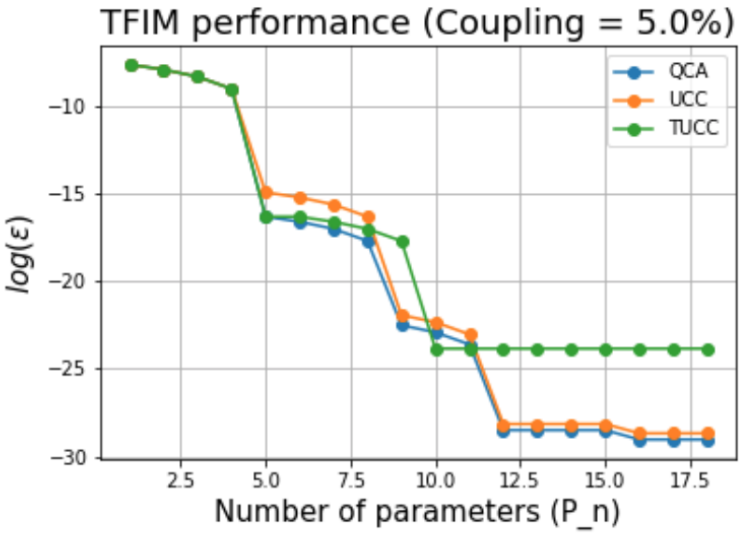

Figure 3.3: *The performance of QCA, TUCC and UCC on a weakly coupled gapped system. In this figure the natural logarithm of the error $log(\epsilon)$ is graphed as a function of the number of parameters used in the ansatz. The ansatzes are applied on a $N = 6$ TFIM system with a coupling of 5% ($C = 0.05$), at which TFIM is gapped (see fig. (2.1a)).*

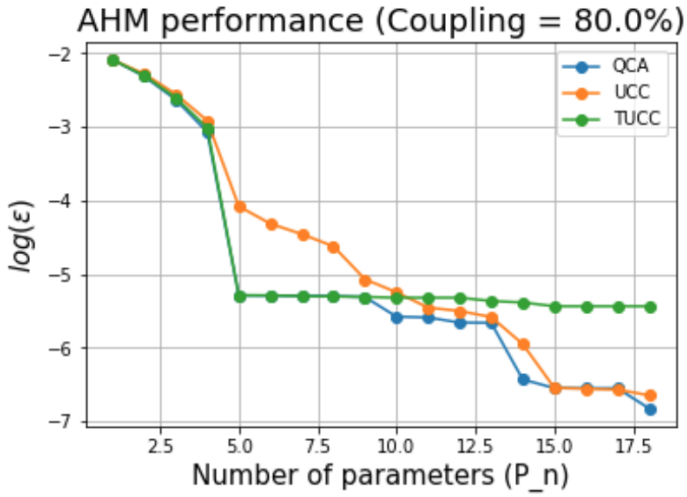

(a) *Anisotropic Heisenberg model*

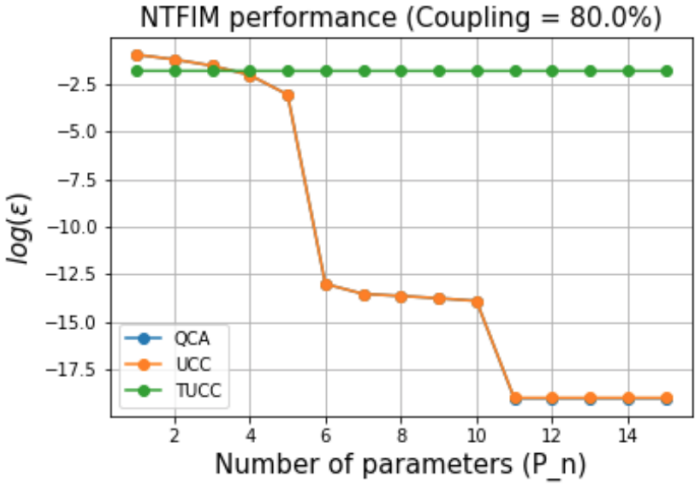

(b) *Non-transverse field Ising model*

Figure 3.4: *The performance of QCA, TUCC and UCC on strongly coupled gapped systems. In these figures the natural logarithm of the error $log(\epsilon)$ is graphed as a function of the number of parameters used in the ansatz. In figure **(a)**, the ansatzes are applied on a $N = 6$ AHM system with a coupling of 80% ($C = 0.8$), at which AHM is gapped (see fig. (2.1b)). **(b)** shows the performances of the ansatzes as applied to a 6 qubit NTFIM system with a coupling of 80% (C = 0.8). This model is also gapped (see fig. (2.1c)). Note that the performance of QCA and UCC coincide.*

Version of June 19, 2020– Created June 19, 2020 - 18:30

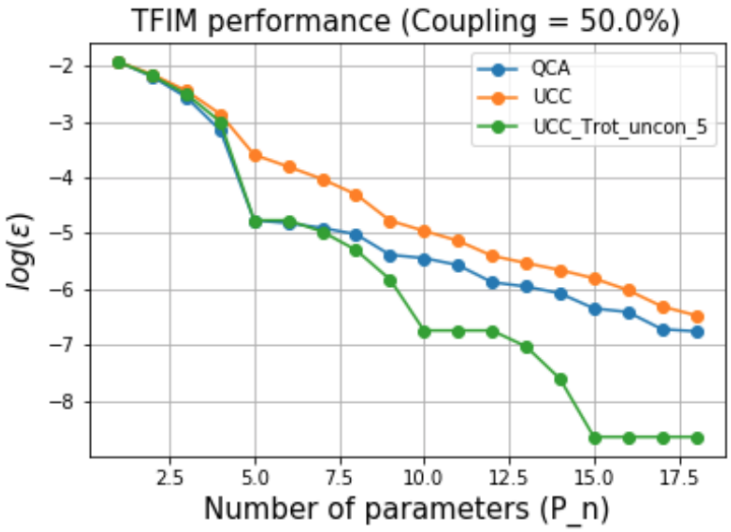

Figure 3.5: *The performance of QCA, UCC and TUCC for a strongly coupled gapped system. In this figure the natural logarithm of the error $log(\epsilon)$ is graphed as a function of the number of parameters used in the ansatz. TUCC is represented by the green line (UCC_Trot_uncon_5).*

One can see that QCA typically outperforms TUCC in weakly coupled gapped systems. In this regime, perturbation theory generally is applicable. Since QCA is able to reproduce perturbation theory, QCA unsurprisingly performs best. TUCC on the other hand doesn't satisfy the linked cluster theorem. Therefore we cannot expect TUCC to reproduce perturbation theory.
For systems strongly coupled and gapless systems, perturbation theory is not applicable anymore. The ground state is not adiabatically connected to the unperturbed ground state, such that perturbation theory breaks down. In those regimes, we observe that TUCC outperforms QCA.
Although perturbation theory is inaccurate for strongly coupled systems, we observe that QCA outperforms TUCC at strongly coupled gapped systems. This result is in line with our expectation, as the ground state is adiabatically connected to the unperturbed ground state.
Based on these observations, we provide a system-adapted criterion for Trotterization choice. If the system is adiabatically connected to the unperturbed ground state, N_P gates of the QCA outperform N_P gates of TUCC. If the system is gapless or adiabatically disconnected from the unperturbed ground state, N_P gates of TUCC will perform superior to N_P gates of QCA.

Version of June 19, 2020– Created June 19, 2020 - 18:30

3.1.4 Changing angles

To investigate the functioning of TUCC and QCA, we plot the values of the optimized parameters as a function of the number of gates.

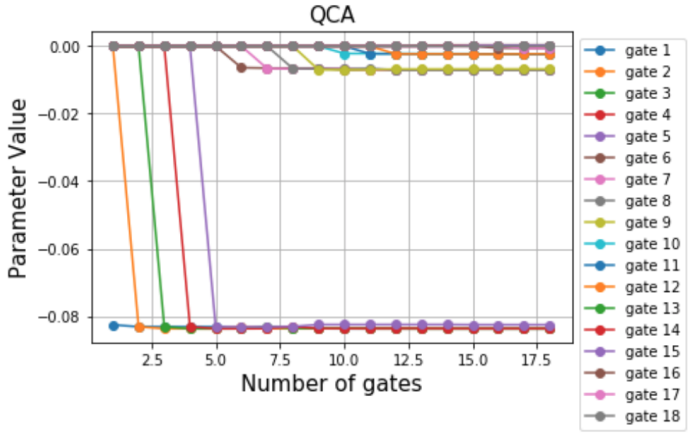

(a) *Optimized parameters QCA*

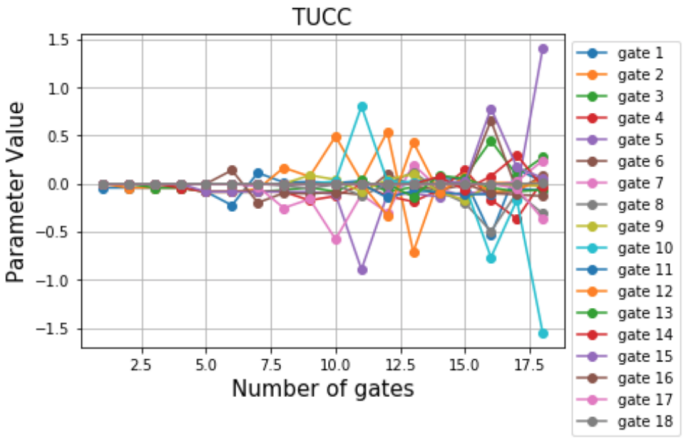

(b) *Optimized parameters TUCC ansatz*

Figure 3.6: *The optimized parameters as a function of the number of gates. In these figures, we consider 18 gates. Each line represents the value of an optimized parameter corresponding to the gate mentioned in the legend. Initially, all parameters are constrained to 0 $\theta_i = 0$. With the increase of the number of gates from $i-1$ to i, θ_i becomes unconstrained. We consider a 6 qubit TFIM, with a coupling of 25 % (C = 0.25). Figure* ***(a)*** *shows the optimized parameters of QCA applied on this model. Whereas figure* ***(b)*** *shows the optimized angles of TUCC for the same model. The TUCC structure consists of repeating first order gates. 6 qubit TFIM has 5 first order contributions, such that the i^{th} parameter and the $(i+5)^{th}$ parameter correspond to similar gates.*

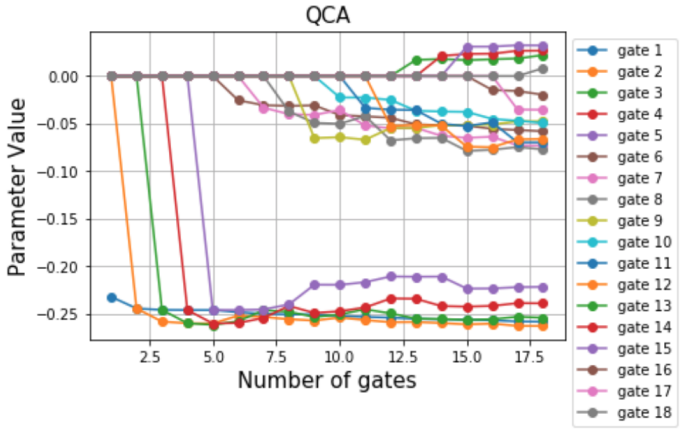

(a) *Optimized parameters QCA*

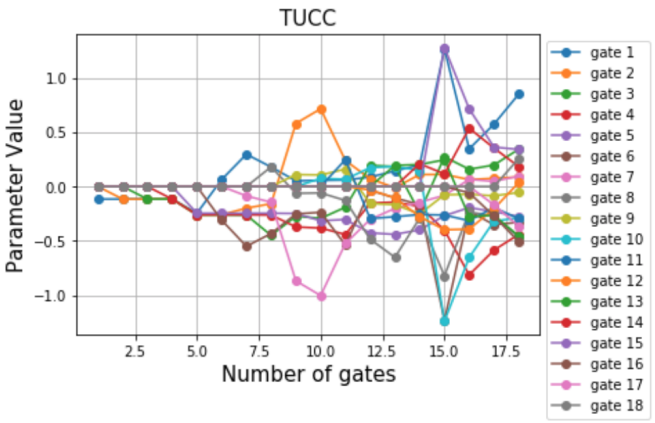

(b) *Optimized parameters TUCC ansatz*

Figure 3.7: *The optimized parameters as a function of the number of gates. In these figures, we consider 18 gates. Each line represents the value of an optimized parameter corresponding to the gate mentioned in the legend. Initially, all parameters are constrained to 0 $\theta_i = 0$. With the increase of the number of gates from $i-1$ to i, θ_i becomes unconstrained. We consider a 6 qubit TFIM, with a coupling of 50 % (C = 0.5). Figure* ***(a)*** *shows the optimized parameters of QCA applied on this model. Whereas figure* ***(b)*** *shows the optimized angles of TUCC for the same model. The TUCC structure consists of repeating first order gates. 6 qubit TFIM has 5 first order contributions, such that the i^{th} parameter and the $(i+5)^{th}$ parameter correspond to similar gates.*

The angles of the gates of QCA behave structured, especially for weakly coupled models. More specifically:

- The optimal angles bunch, forming big groups around just a few dif-

ferent values.

- When new gates are introduced, the old angles are not significantly modified.

These features can be explained with perturbative equations for the QCA angle parameters [8]. These imply, that the main contribution to any angle is defined by the respective leading order connected diagram. This can be used to explain the bunching of optimal angle values. For this, note that the considered spin chain models possess translational symmetry - up to the chain truncation. This implies that multiple diagrams in the perturbative series have the same value, thus explaining the bunching of optimal angles. On the other hand, the perturbative equations for an optimal QCA angle show that the values of other ansatz angles do not have the influence at the leading order. This explains why the angles are not significantly modified when new gates are added to the ansatz.

The applicability of perturbative equations, naturally, is limited to the weakly coupled models. As a result, one would expect the breakdown of the QCA angle structure at strong coupling. This is confirmed by numerics: for strongly coupled models, we see that the parameters of QCA change in a more chaotic way.

The parameters of the TUCC ansatz change more chaotically and disorderly. With the addition of a new gate, other gates often change drastically. One can also observe a certain structure, where angles corresponding to the same generator change in opposite directions, which typically lasts before a single new gate is added. This pattern can be deduced from the analytics that describes the operation of the circuit as a function of the parameters $\vec{\theta}$. For simplicity, let us consider a piece of TUCC of the following form:

$$U(\vec{\theta})\,|\vec{0}\rangle = ..e^{i\theta_1 G_1}e^{i\theta_2 G_2}e^{i\theta_3 G_1}e^{i\theta_4 G_2}..\,|\vec{0}\rangle\,, \tag{3.1}$$

where G_1 and G_2 anti-commute, and .. represents other gates that might be present in TUCC. We will limit our considerations to this example, as it is relatively general and gives enough insight to analyze the features of interest. For small angles θ_i, this can be Taylor expanded as:

$$..(1 + i(\theta_1 + \theta_3)G_1 + i(\theta_2 + \theta_4)G_2 + (\theta_2(\theta_1 - \theta_3) + \theta_4(\theta_1 + \theta_3))i^2 G_1 G_2).. \left|\vec{0}\right\rangle \tag{3.2}$$

$$= \left|\vec{0}\right\rangle + (\theta_1 + \theta_3)\left|\vec{s}_1\right\rangle + (\theta_2 + \theta_4)\left|\vec{s}_2\right\rangle + (\theta_2(\theta_1 - \theta_3) + \theta_4(\theta_1 + \theta_3))\left|\vec{s}_3\right\rangle + .., \tag{3.3}$$

for $\left|\vec{s}_1\right\rangle = iG_1\left|\vec{0}\right\rangle$, $\left|\vec{s}_2\right\rangle = iG_2\left|\vec{0}\right\rangle$, $\left|\vec{s}_3\right\rangle = i^2 G_1 G_2\left|\vec{0}\right\rangle$, and $+..$ representing other possible contributions. Let us assume that the considered part of TUCC has to reproduce the state of the following form:

$$\left|\Psi\right\rangle = \left|\vec{0}\right\rangle + C_1\left|\vec{s}_1\right\rangle + C_2\left|\vec{s}_2\right\rangle + C_3\left|\vec{s}_3\right\rangle + .., \tag{3.4}$$

For some real coefficients $C_{1,2,3} \in \mathbb{R}$. Let us compare (3.3) and (3.4) while consecutively including the gates to the ansatz. Specifically, let us allow nonzero values for angles θ_i, increasing i from 1 to 4. With $\theta_{1,2} \neq 0$, we are able to reproduce the contributions proportional to $C_{1,2}\left|\vec{s}_{1,2}\right\rangle$: $C_{1,2} \approx \theta_{1,2}$. We may also hope that $C_3 = \theta_1\theta_2$ and thus is automatically reproduced. However, this cannot be guaranteed, as $\theta_{1,2}$ is already fixed by $C_{1,2}$. When θ_3 is introduced on top, two changes occur. On the one hand, C_3 can now be reproduced using this new degree of freedom: $C_3 = \theta_2(\theta_1 - \theta_3)$. On the other hand, we now demand: $C_1 = \theta_1 + \theta_3$. This means that rather than θ_1 and θ_3, the linear combinations $\theta_1 \pm \theta_3$ more directly represent the coefficients $C_{1,3}$. This observation allows us to understand the 'opposite angle' feature, typical in the TUCC angle plots. Using the notation of this example, this feature means that $\theta_1 + \theta_3$ is much smaller than $\theta_1 - \theta_3$. This is not too surprising, as it is clear now that these contribute to different terms and thus may significantly differ. One last question is: why does this feature disappear when new angles are introduced? In the example above, this corresponds to the inclusion of θ_4: now $C_2 = \theta_2 + \theta_4$, $C_3 = \theta_2(\theta_1 - \theta_3) + \theta_4(\theta_1 + \theta_3)$. For nonzero θ_4, $\theta_1 \pm \theta_3$ now stops being independent variables, and thus the same state can be represented in a way not requiring nearly-opposite $\theta_{1,3}$. This concludes our analysis of the features in TUCC angle plot. To explain the chaotic behavior in TUCC angles, let us consider including more contributions to the ground state. From the example above, it is clear that for this, one needs to introduce more gates and expand to a higher order in θ_i. The respective equations quickly get highly non-linear, which qualitatively explains the chaotic behavior of the angles.

Note that the angles of TUCC change chaotically even if the performance doesn't improve as more gates are added to the VQE. This might indicate the presence of barren plateaus [10]. Barren plateaus occur when the landscape in which the angles settle is flat. In this case, the angles wander around the plateau without improving the performance.

3.1.5 Hessians

In order to investigate the landscape of $E(\vec{\theta})$ in which the optimized parameters settle, we examine the eigenvalues of the Hessians. The Hessian at minimum $\vec{\theta}_{min}$ is given by:

$$\mathcal{H}_{ij} = \frac{\partial E(\vec{\theta}_{min})}{\partial\theta_i \partial\theta_j}, E(\vec{\theta}) = \langle U(\vec{\theta})\vec{0}| \, H \, |U(\vec{\theta})\vec{0}\rangle \tag{3.5}$$

Derivatives of $|\Psi(\vec{\theta})\rangle = U(\vec{\theta})\,|\vec{0}\rangle$ with respect to any parameter θ_i are easily evaluated due to its periodic nature.

$$\frac{\partial\,|\Psi(\vec{\theta})\rangle}{\partial\theta_\alpha} = e^{i\theta_N P_N}...\frac{\partial e^{i\theta_\alpha P_\alpha}}{\partial\theta_\alpha}...e^{i\theta_1 P_1}\,|\vec{0}\rangle$$

The derivative of the exponential simplifies to:

$$\frac{\partial e^{i\theta_\alpha P_\alpha}}{\partial\theta_\alpha} = iP_\alpha e^{i\theta_\alpha P_\alpha}$$

But $iP_\alpha = e^{i\frac{\pi}{2}P_\alpha}$, which gives:

$$\frac{\partial\,|\Psi(\vec{\theta})\rangle}{\partial\theta_\alpha} = |\Psi(\vec{\theta} + \vec{\delta_\alpha}\frac{\pi}{2})\rangle \equiv |\Psi\rangle^{(\alpha)}$$

Where $\vec{\delta_\alpha}$ is a vector with zeros at all entries, except for position α, which is given by a one. To make the notation more convenient, we define $|\Psi(\vec{\theta} + \vec{\delta_\alpha}\frac{\pi}{2})\rangle$ as $|\Psi\rangle^{(\alpha)}$. Now the derivative of $E(\vec{\theta}) = \langle\Psi|\,H\,|\Psi\rangle$ with respect to θ_α becomes:

$$\frac{\partial E(\vec{\theta})}{\partial\theta_\alpha} = \langle\Psi|\,H\,|\Psi\rangle^{(\alpha)} + \langle\Psi|^{(\alpha)}\,H\,|\Psi\rangle = 2\,\mathrm{Re}(\langle\Psi|\,H\,|\Psi\rangle^{(\alpha)})$$

Such that the resulting Hessian is of the form:

$$\mathcal{H}_{\alpha\beta} = 2\,\mathrm{Re}(\langle\Psi|\,H\,|\Psi\rangle^{(\alpha,\beta)}) + 2\,\mathrm{Re}(\langle\Psi|^{(\beta)}\,H\,|\Psi\rangle^{(\alpha)}) \tag{3.6}$$

We consider eigenvalues of this Hessian, evaluated at a particular minimum $\vec{\theta_{min}}$, by calculating a geometric average. This quantity gives a measure of the curvature of the landscape. This is done in the following way:

$$C = \sqrt[N_p]{\Pi_i^{N_p} \lambda_i} \tag{3.7}$$

Where λ_i are the eigenvalues of the regarding Hessian and where N_p represents the number of parameters. For barren plateaus, the landscape is expected to be flat. We found that the the geometric averages of the eigenvalues C in the local minimums of TUCC in the chaotic non-improving regime, are 3 to 5 times smaller compared to QCA. This result shows the landscape of TUCC to be considerably flatter. The presence of barren plateaus however, cannot be concluded from this result.

Version of June 19, 2020– Created June 19, 2020 - 18:30

3.1.6 Increasing coupling strength

Another way of studying the ansatzes is to examine their behaviors while the coupling strength gradually increases. We investigate both the behavior of the angles, as well as the performance. Because the TFIM model possesses a critical point at $J = 1$, one can expect to observe drastic change in the angles and the performance. NTFIM and AHM will naturally change more smoothly, as the models stay gapped for finite values of coupling J.

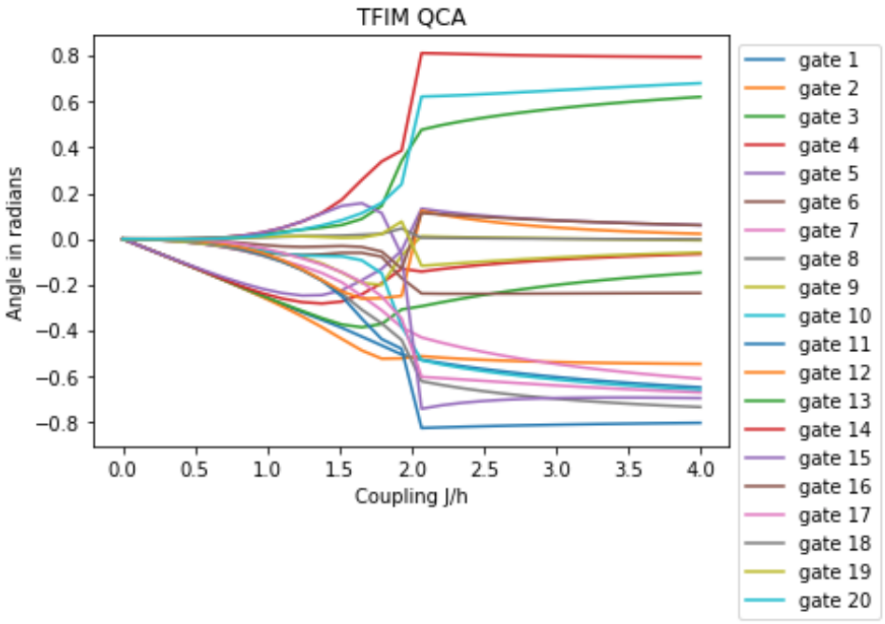

Figure 3.8: *Optimized parameters for QCA on TFIM as the coupling J increases. We consider 20 gates. As the coupling J increases, the Hamiltonian changes. Therefore the optimized angles shift. In this figure, we consider a 6 qubit TFIM system where we increase the coupling from $J = 0$ to $J = 4$.*

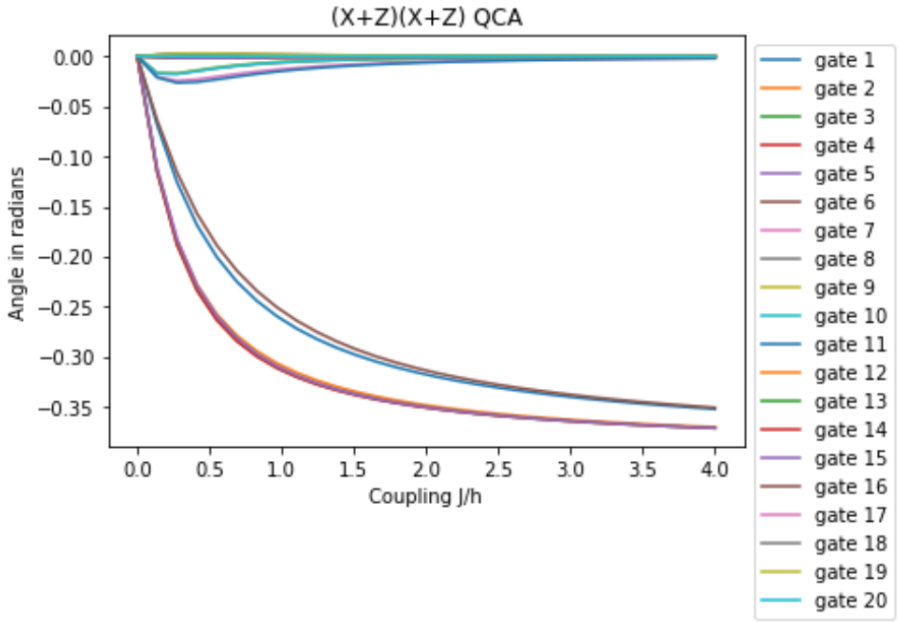

Figure 3.9: *Optimized parameters for QCA on TFIM as the coupling J increases. We consider 20 gates. As the coupling J increases, the Hamiltonian changes. Therefore the optimized angles shift. In this figure, we consider a 6 qubit NTFIM system where we increase the coupling from $J = 0$ to $J = 4$.*

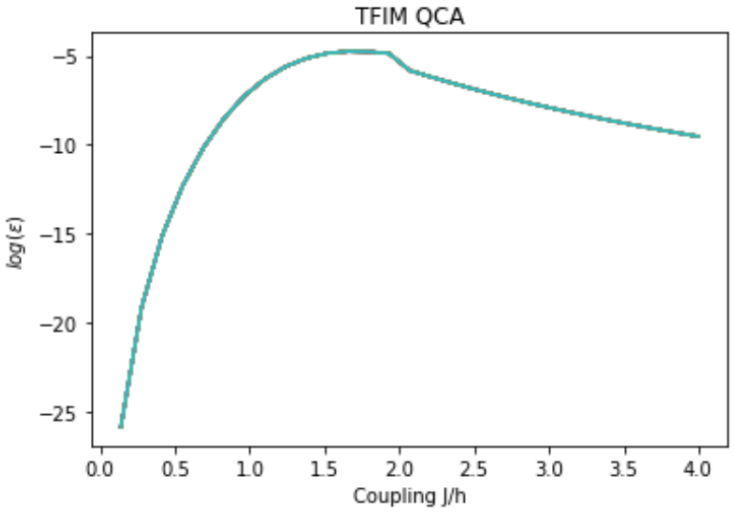

Figure 3.10: *Performance of QCA on 6 qubit NTFIM as a function of coupling J. In this figure, the y-axis yields the natural logarithm of the error ϵ by a 20-gate QCA. The coupling on the x-axis reaches from $J = 0$ to $J = 4$*

Version of June 19, 2020– Created June 19, 2020 - 18:30

As predicted, one can notice a drastic change in the angles for the TFIM model in fig.(3.8). The point at which this change occurs however, does not correspond to $J = 1$, the position of the gap closing (see fig. (2.1a)). This difference is found to be nontrivial and applies as material for future study. The parameters of the QCA ansatz applied on a NTFIM do not encounter a sudden change as the coupling becomes stronger (fig. (3.9)). Furthermore, one can see that the performance initially gets worse as the coupling strength increases (fig. (3.10)). After $J = 2$, the performance improves again. The ansatzes typically perform worst at couplings strengths $J \sim 1$. In this regime, the interacting part and the non-interacting part contribute roughly equally to the total Hamiltonian. In this case, the corresponding ground state of this Hamiltonian is maximally entangled. Therefore, more gates are required to map the initial state to this ground state. Which results in a relatively big error in the energy.

3.2 Heuristic

3.2.1 Sharp-shooting and chaotic search

The QCA ansatz satisfies the linked cluster theorem and consists of all different gates based on perturbation theory. This ansatz is built to efficiently reach the ground-state according to perturbation theory. As more gates are added to the VQE, the parameters generally change in a structured way (see fig. (3.6a) (3.7a). Especially when perturbation theory is considered as an accurate approximation. In this regime, the performance of QCA is generally superior to that of TUCC (see fig. (3.3)). We say that QCA "sharp-shoots" towards the part of the Hilbert space where the ground state according to perturbation theory is located.
For strongly coupled gapless systems however, we see that TUCC performs better than QCA (see fig. (3.6b)(3.7b)). In this regime, perturbation theory predicts the ground state less accurately. Consequently, the structure of QCA is not ideally constructed to reach the ground state. Or in other words, the "sharp-shooting" mechanism points in the wrong direction.
TUCC on the other hand, does not depend on perturbation theory as much as QCA does, since it doesn't satisfy the linked cluster theorem. Instead, TUCC relies on its non-linearity, due to the repetition of similar low-entangling gates. TUCC as applied to the initial state $|\vec{0}\rangle$ therefore mostly produces low entanglement states. From this, we conclude TUCC more thoroughly explores through the region in the Hilbert space of low entanglement states.

We say TUCC is a better "chaotic searcher" than QCA, since QCA also possesses non-local, relatively entangling gates.

3.2.2 Geometrical evidence

In order to provide the heuristic with evidence, we perform a numerical experiment, which shows TUCC to be a more efficient chaotic searcher. This is done by showing that TUCC produces more non-overlapping low entanglement states than QCA.
First, a large number of random combinations of parameters $\vec{\theta}_{random}$ are chosen. Each random combination produces a state according to QCA and a state according to TUCC.

$$|\Psi_{QCA}\rangle = U_{QCA}(\vec{\theta}_{random})\,|\vec{0}\rangle$$

$$|\Psi_{TUCC}\rangle = U_{TUCC}(\vec{\theta}_{random})\,|\vec{0}\rangle$$

For each state, the entanglement entropy is determined. The entanglement entropy of a system with density matrix ϱ_{AB}, divided into system A and B is given by:

$$S(\varrho_A) = -\operatorname{Tr}(\varrho_A \log(\varrho_A))$$

Where ρ_A is the partial trace of ρ_{AB} with respect to system B: $\rho_A = \operatorname{Tr}_B(\varrho_{AB})$. We take the first qubit to be subsystem A, such that the remaining qubits form subsystem B. We expect that the states produced by TUCC are less entangled. Hypothesis: TUCC* covers the volume in the vicinity better than QCA
To exclude the possibility that the states that TUCC outputs are more overlapping compared to QCA, the distance between the states is measured and compared to QCA. We calculate this as follows:

$$AverageDistance = \frac{1}{n(n-1)} \sum_{i}^{n-1} \sum_{j=i+1}^{n} \operatorname{norm}(\psi_i - \psi_j)$$

Where n is the total number of states produces by the circuit. The results show that the average distance between the states is similar for TUCC and QCA.

	QCA	TUCC
Average entropy	0.605	0.513
Average distance	1.424	1.410

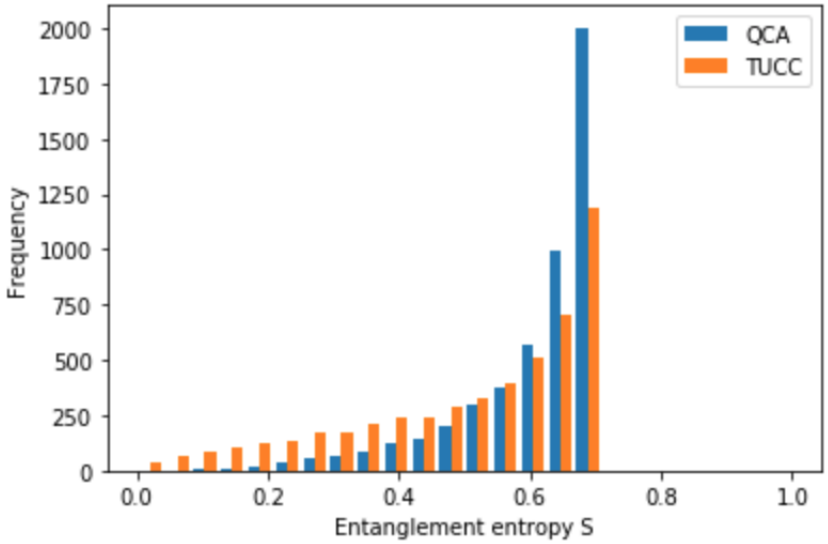

Figure 3.11: *Histogram of the entanglement entropy of states $\psi \in \mathbb{C}^{2^6}$ produced by 15-gate QCA circuit and a 15-gate TUCC circuit. 5000 random combinations of angles are used to produce the quantum states. Thereafter, the entanglement entropy of the first qubit compared to the other 5 is measured. The frequency on the y-axis yields the number of times a quantum state returns that particular value of entanglement entropy S.*

The results show that TUCC produces states that are on average less entangled. So, when perturbation theory is inapplicable, the ansatzes search chaotically. We conclude this is done most efficiently by TUCC.

Chapter 4

Hybrid-ansatz

Based on the heuristic made on QCA and TUCC, we introduce a hybrid ansatz. The first gates of this ansatz are structured in the same way as the QCA ansatz. After a certain amount of gates, the structure switches to a TUCC type ansatz. With this composite ansatz, the QCA gates efficiently reach a state in the vicinity of the ground state according to perturbation theory. Thereafter, the TUCC gates effectively search for the actual ground state by a chaotic exploration of surrounding states. We expect this ansatz to be most successful for systems that are still related to perturbation theory, but are already vastly different. In this regime, both QCA and TUCC are relatively unsuccessful. By combining the strengths of the two, an improvement of performance is observed.
From the figures (fig. (4.1-4.5)), one can see that QCA outperforms the hybrid ansatz for the weakly coupled system (C = 5%). For C = 25%, TUCC, QCA and the hybrid ansatz perform similarly. For TFIM at the critical point however (fig. (4.3)), the hybrid ansatz performs considerably better compared to both QCA and TUCC. For C = 80%, the hybrid ansatz is slightly preferred over TUCC.

4.1 Performance

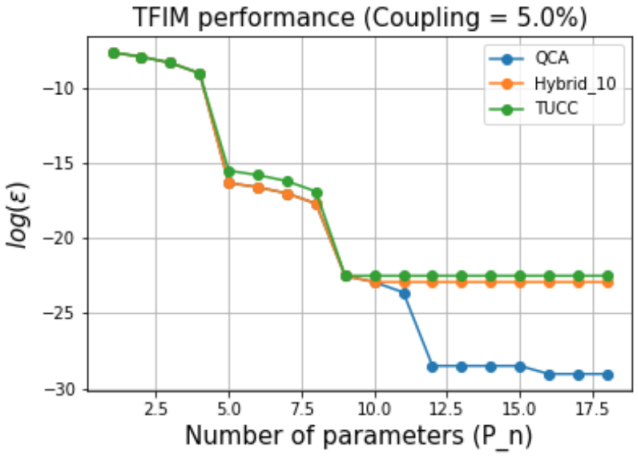

Figure 4.1: *The performance of QCA, TUCC and the hybrid ansatz on a weakly coupled gapped system. In this figure the natural logarithm of the error $log(\epsilon)$ is graphed as a function of the number of parameters used in the ansatz. The ansatzes are applied on a $N = 6$ TFIM system with a coupling of 5% ($C = 0.05$). The Hybrid ansatz switches from a QCA to a TUCC scheme at the 10^{th} gate.*

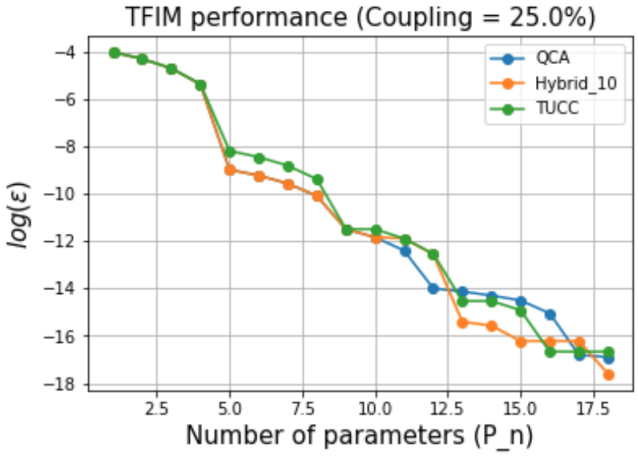

Figure 4.2: *The performance of QCA, TUCC and the hybrid ansatz. In this figure the natural logarithm of the error $log(\epsilon)$ is graphed as a function of the number of parameters used in the ansatz. The ansatzes are applied on a $N = 6$ TFIM system with a coupling of 25% ($C = 0.25$). The Hybrid ansatz switches from a QCA to a TUCC scheme at the 10^{th} gate.*

Version of June 19, 2020– Created June 19, 2020 - 18:30

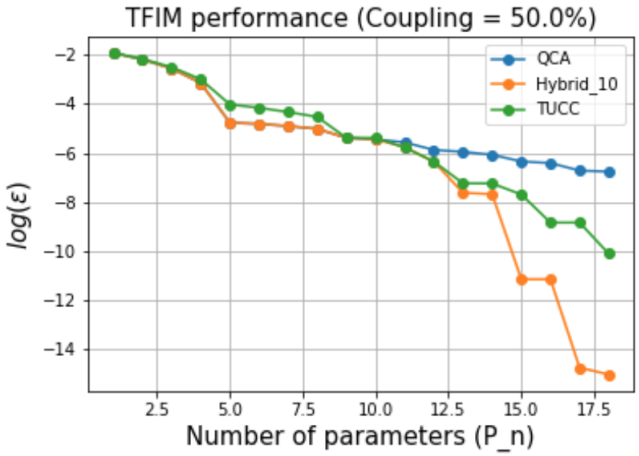

Figure 4.3: *The performance of QCA, TUCC and the hybrid ansatz applied on TFIM at the critical point $J = 1$. In this figure the natural logarithm of the error $log(\epsilon)$ is graphed as a function of the number of parameters used in the ansatz. The ansatzes are applied on a $N = 6$ TFIM system with a coupling of 50% ($C = 0.5$). The Hybrid ansatz switches from a QCA to a TUCC scheme at the 10^{th} gate.*

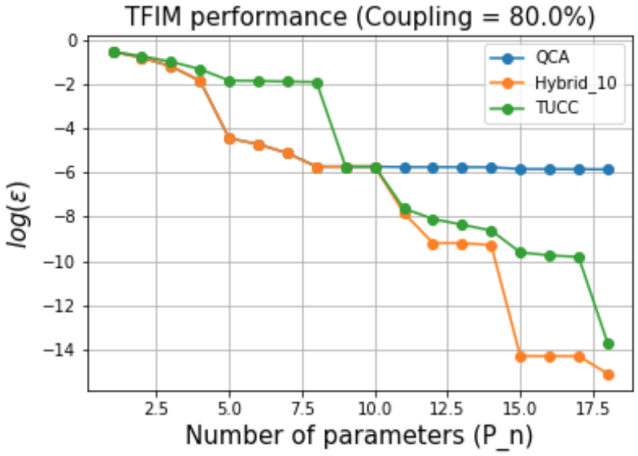

Figure 4.4: *The performance of QCA, TUCC and the hybrid ansatz on a strongly coupled gapless system. In this figure the natural logarithm of the error $log(\epsilon)$ is graphed as a function of the number of parameters used in the ansatz. The ansatzes are applied on a $N = 6$ TFIM system with a coupling of 80% ($C = 0.8$). The Hybrid ansatz switches from a QCA to a TUCC scheme at the 10^{th} gate.*

Version of June 19, 2020– Created June 19, 2020 - 18:30

Chapter 5

Conclusion

In this project we have investigated different UCC-based ansatz schemes for variational quantum eigensolvers (VQEs), applied on spin systems. An ansatz is specified by a selection of generators and the choice of Trotterization scheme. These variables essentially determine the effectiveness of the ansatz. Choosing these variables carefully, might therefore be critical for quantum advantage in the near future. A standard approach in UCC theory is to choose generators motivated by perturbation theory. On the same note, we constructed a Python module that returns a desired number of generators based on perturbation theory. With the generator choice being set, we identified two tendencies in the Trotterization scheme: Either Trotterize with one Trotter step $\rho = 1$ (QCA), or use multiple Trotter steps, only repeating the first order gates (TUCC). When we compared these ansatzes among various models, we found their performances to be drastically different. Based on the results, we suggest that QCA performs superior to TUCC for weakly coupled, and strongly coupled gapped, systems. For gapless systems however, we suggest that TUCC outperforms QCA. By examining the optimized parameters as gates are added, we observe that the parameters of QCA behave more structured compared to the parameters of TUCC. The angles of TUCC seem to change chaotically with the addition of a new gate, even if the performance of the ansatz does not improve. This result motivates to inspect the landscape of $E(\vec{\theta})$, which is done by a study of the Hessians. This showed that the landscape of TUCC is typically less curved compared to the landscape of QCA. Based on these results, we provided a heuristic about the characteristics of QCA and TUCC: QCA effectively reproduces the ground state accord-

ing to perturbation theory, whereas TUCC is an efficient chaotic searcher. This statement is substantiated by a numerical experiment, showing that TUCC produces more low entanglement states than UCC. At last, we proposed a composite ansatz of QCA and TUCC motivated by the heuristic. This new ansatz is found to outperform both QCA and TUCC, especially for systems with a coupling J around the critical point $J_{critical}$. With the addition of this result, we present the following system-adapted criterion for Trotterization choice: QCA performs best for systems that are adiabatically connected to the unperturbed ground state. Otherwise, when the ground state is adiabatically disconnected from the unperturbed ground state, either TUCC or the hybrid ansatz is suggested. More specifically, for systems with $J \sim J_{critical}$, the hybrid ansatz is preferred. Due to the drastically different performances of the ansatzes depending on the system, we recognize the cruciality of the Trotterization choice for quantum advantage in the near future. Therefore, further study of different ansatzes and other systems is of importance.

Version of June 19, 2020– Created June 19, 2020 - 18:30

Bibliography

[1] R. P. Feynman, International Journal of Theoretical Physics **21**, 467 (1982).

[2] J. Preskill, Quantum **2** (2018).

[3] J. R. McClean, J. Romero, R. Babbush, and A. Aspuru-Guzik, New J. Phys. **18**, 023023 (2016).

[4] D. I. Lyakh, M. Musiał, V. F. Lotrich, and R. J. Bartlett, Chem. Rev. **112**, 182 (2011).

[5] K. A. Brueckner, Phys. Rev. **100**, 36 (1955).

[6] H. F. Trotter, Proc. Ams. Math. Soc. **10**, 545 (1959).

[7] M. Suzuki, J. Math. Phys. **32** (1991).

[8] Y. Herasymenko and T. E. O'Brien, (2019), arXiv:1907.08157 .

[9] J. Kirkwood and L. Thomas, Commun. Math. Phys. **88**, 569 (1983).

[10] J. McClean, S. Boixo, V. Smelyanskiy, R. Babbush, and H. Neven, Nat. Comm. **9**, 4812 (2018).